Accepted Manuscript

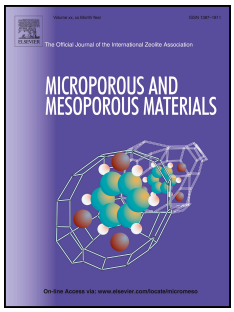

UHMWPE/SBA-15 nanocomposites synthesized by *in situ* polymerization

Ana E. Ferreira, Maria L. Cerrada, Ernesto Pérez, Vicente Lorenzo, Henri Cramail, João P. Lourenço, M. Rosário Ribeiro

PII: S1387-1811(16)30196-2

DOI: 10.1016/j.micromeso.2016.06.002

Reference: MICMAT 7744

To appear in: *Microporous and Mesoporous Materials*

Received Date: 16 March 2016

Revised Date: 11 May 2016

Accepted Date: 1 June 2016

Please cite this article as: A.E. Ferreira, M.L. Cerrada, E. Pérez, V. Lorenzo, H. Cramail, J.P. Lourenço, M.R. Ribeiro, UHMWPE/SBA-15 nanocomposites synthesized by *in situ* polymerization, *Microporous and Mesoporous Materials* (2016), doi: 10.1016/j.micromeso.2016.06.002.

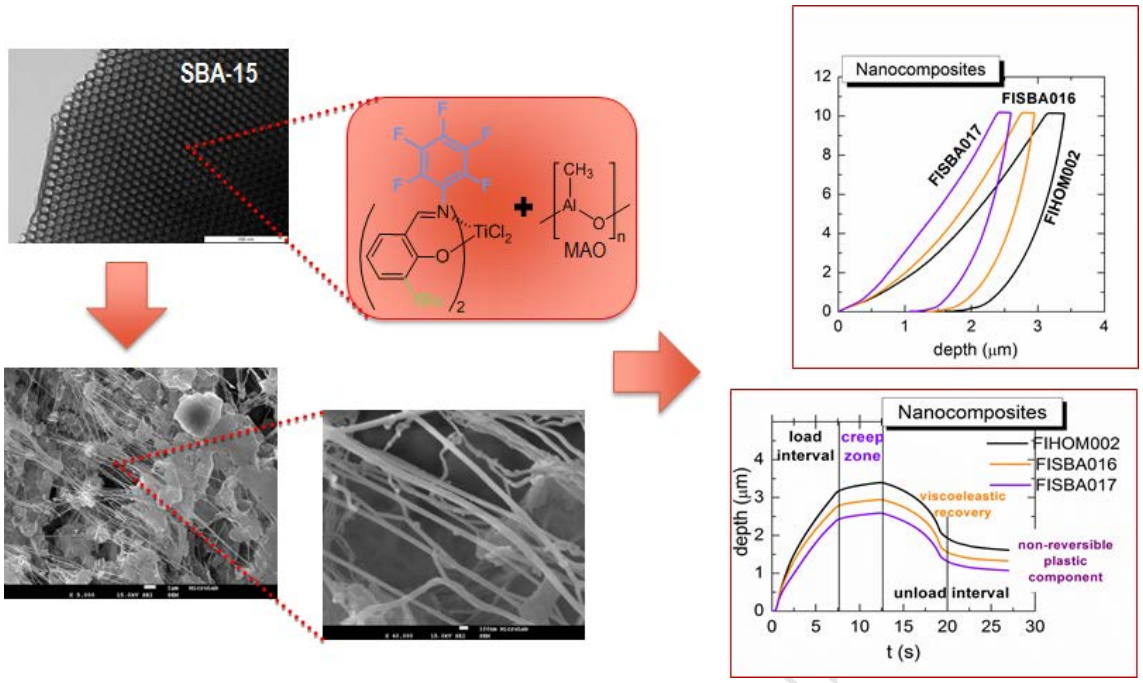

UHMWPE/SBA-15 nanocomposites synthesized by *in situ* polymerization

Ana E. Ferreira[a,b], Maria L. Cerrada[c]*, Ernesto Pérez[c], Vicente Lorenzo[d], Henri Cramail[b], João P. Lourenço[a,e], M. Rosário Ribeiro[a]*

[a] Centro de Química Estrutural & Instituto Superior Técnico, Universidade de Lisboa, Av. Rovisco Pais, Lisboa, Portugal

[b] Laboratoire de Chimie des Polymères Organiques, UMR5629, Université Bordeaux, CNRS, INP-Bordeaux-ENSCBP, 16, Avenue Pey Berland, Pessac Cedex, F-33607, France

[c] Instituto de Ciencia y Tecnología de Polímeros (ICTP-CSIC), Juan de la Cierva 3, 28006 Madrid, Spain

[d] Grupo de Investigación "POLímeros: Caracterización y Aplicaciones" (U. A. del ICTP-CSIC), E.T.S.I. Industriales, Universidad Politécnica de Madrid, José Gutiérrez Abascal 2, 28006 Madrid, Spain

[e] Faculdade de Ciências e Tecnologia, CIQA, Universidade do Algarve. Campus de Gambelas, 8005-139 Faro, Portugal

*Corresponding authors: E-mail addresses: rosario@tecnico.ulisboa.pt (M.R. Ribeiro) mlcerrada@ictp.csic.es (M.L. Cerrada);

Abstract

Different nanocomposites have been attained by *in situ* polymerization based on ultra-high molecular weight polyethylene (UHMWPE) and mesoporous SBA-15, this silica being used for immobilization of the FI catalyst bis [*N*-(3-*tert*-butylsalicylidene)-2,3,4,5,6-pentafluoroanilinato] titanium (IV) dichloride and as filler as well. Two distinct approaches have been selected for supporting the FI catalyst on the SBA-15 prior polymerization. A study on polymerization activity of this catalyst has been performed

under homogenous conditions and upon heterogenization. A study of the effect of presence of mesoporous particles and of the immobilization method is also carried out. Moreover, the thermal characterization, phase transitions and mechanical response of some pristine UHMWPEs and UHMWPE / SBA-15 materials have been carried out. Relationships with variations on molar mass, impregnation method of catalyst and final SBA-15 content have been established.

Keywords: UHMWPE; nanocomposites; mesoporous SBA-15; FI catalyst; immobilization approaches.

1. Introduction

Ultra-high molecular weight polyethylene (UHMWPE) is a very attractive thermoplastic polymer due to its remarkable physical and mechanical properties, such as high chemical and abrasion resistance, good corrosion performance, high impact toughness, resistance to cyclic fatigue, and resistance to radiation [1-3]. Moreover, it is widely used in medical device applications (e.g. hip and knee prostheses and joint replacements) because of its biocompatibility, high mechanical strength, low fatigue and wear characteristics [4, 5].

These comprehensive uses justify the ongoing demand for UHMWPE with tailored mechanical and/or thermal behavior and has urged the development of methods to improve its properties, for instance the blending of UHMWPE with other polymers, mineral particles, or the addition of reinforcement agents [6, 7]. Several studies have been made related to the incorporation of fillers, like CNTs [8, 9], carbon fibers [10], or even UHMWPE fibers, leading in this latter case to self-reinforced UHMWPE composites [11]. Relative small amounts (<3 wt.%) of inorganic particles, such as silica, titania, or calcium carbonate having dimensions in the nanometer scale, have been proven to increase both rigidity and toughness of several thermoplastics [12, 13]. As an example, an improvement in tensile modulus and impact strength was observed for high-density polyethylene (HDPE)/silica nanocomposite [14].

Properties of nanocomposites depend, in general, on the nature and distribution of the nanofillers but also on the fabrication method. Polyethylene (PE) nanocomposites are mostly produced by the conventional method of physical blending. Nevertheless, one of the crucial drawbacks of UHMWPE is its extremely high melt viscosity, which hinders the use of these traditional processing techniques [15]. Due to its very high molecular weight and, consequently, entanglement density, the mobility of the UHMWPE chains is limited and the complete melting of the polymer during its processing is hardly achieved, leading to a heterogeneous final product with fusion defects and/or grain-

boundaries. Furthermore, an effective dispersion of nanofillers throughout the UHMWPE polymeric matrix would turn out rather difficult by using those conventional methods, leading to poor mechanical and thermal properties in the resulting nanocomposites.

An alternative approach for fabrication of homogenously dispersed nanocomposites is *in situ* polymerization where a good dispersion of the fillers can be obtained, as well as a more effective interaction between the filler particles and the polymer matrix [8, 16]. Kaminsky *et al.* [16] produced UHMWPE/multiwalled carbon nanotube (MWCNT) nanocomposites by using *in situ* polymerization with a metallocene catalyst, Sánchez *et al*. [9] reported the preparation of UHMWPE/MWCNT nanocomposite using a $TpTiCl_2(Et)$ system and Park and Choi [17] attained UHMWPE/MWCNT nanocomposites by using half-titanocene catalytic system.

Ordered mesoporous silicas, such as MCM-41 and SBA-15, emerged in the 1990s and show a hexagonal arrangement of uniformly sized cylindrical pores, with a narrow pore size distribution and large surface area [18, 19]. They are well suited for the immobilization of several organometallic complexes. Compared to MCM-41, SBA-15 possesses pores of larger diameter, typically 3 nm for MCM-41 and 7 nm for SBA-15. Moreover, these pores may act as polymerization nanoreactors and affect the pattern of monomer insertion and the polymer morphology. Research papers published in recent years demonstrate the ability of these mesoporous silicas to produce nanometer scaled PE through space confined polymerization [20-22]. Dong *et al.* produced PE nanofibers with Cp_2ZrCl_2 fixed on MCM-41 and SBA-15 where the later fibers possess larger diameters due to the higher SBA-15 pore diameter [23]. After supporting an iron(II)-bisimine pyridine catalyst on SBA-15, Xu *et al.* obtained polyethylene with higher molar mass than its homogeneous counterpart and fibrous morphology [24]. *In situ* supported ethylene polymerization on MCM-41 channels has been recently described as an effective route for the preparation of nanocomposites. Special interactions between the MCM-41 material and the polyethylene are developed [25]

under those confined synthetic conditions. The resulting self-reinforced HDPE/MCM-41 nanocomposites revealed improved mechanical performance and easier degradability at the end of the life cycle [21, 25]. Attempts to improve dispersion of micro or nanosized mesoporous MCM-41 particles within HDPE matrix using the *in situ* polymerization methodologies were reported later on. These methodologies aimed to boost interfacial adhesion between components (HDPE matrix and MCM-41) and involved either the functionalization of HDPE chains by copolymerization with a polar monomer or the modification of MCM-41 surface by several modifying agents before polymerization [26, 27].

Despite all these efforts, the manufacture of homogenously dispersed nanocomposites from UHMWPE is still a challenging task [8]. The present work aims the synthesis of high performance polyolefin nanocomposites, exhibiting an intimate mixing and combining the advantages of using the mesoporous silica SBA-15 with a single-site bis-(phenoxyimine) titanium dichloride catalyst, the bis [*N*-(3-*tert*-butylsalicylidene)-2,3,4,5,6-pentafluoroanilinato] titanium (IV) dichloride (FI catalyst), able to produce UHMWPE. SBA-15 is selected as a suitable support due its large mesoporous channels that could facilitate the access of the titanium complex. Distinct immobilization methodologies and their effect on the polymerization activity are investigated. In addition, preliminary thermal characteristics and mechanical behavior of these nanocomposites are evaluated. The performance of these materials is discussed in terms of morphology and crystalline structure assessed by SEM and DSC.

2. Experimental part

2.1 Materials and chemicals

All the chemicals for the synthesis of the SBA-15 particles, P-123 (poly(ethyleneglycol)-block-poly(propyleneglycol)-block-poly(ethyleneglycol)), hydrochloric acid (37% aq.

sol.), TEOS (tetraethylorthosilicate), NaCl and ethanol, were purchased from Sigma-Aldrich and used as received.

All experiments for the SBA-15 modification and ethylene polymerization were carried out under dry nitrogen using standard Schlenk techniques. Ethylene and nitrogen (Air Liquide) were purified through absorption columns containing molecular sieves 4A and 13X. bis [*N*-(3-*tert*-butylsalicylidene)-2,3,4,5,6-pentafluoroanilinate] titanium (IV) dichloride (FI catalyst, MCAT) and methylaluminoxane (MAO, 7 wt. % Al in toluene solution, AkzoNobel) were used as received. Toluene (VWR Chemicals) was dried by refluxing over metallic sodium under a dry nitrogen atmosphere, using benzophenone as indicator.

2.2 Preparation and characterization of pure SBA-15

The synthesis of pure SBA-15 support was carried out as follows: 13.2 g of P-123 were dissolved in 500 mL of water and kept stirring during the night, at room temperature. The temperature was raised to 40 ℃ and then 45 mL of hydrochloric acid (37% aq. sol.) and 30.8 g of TEOS were added. After ca. 2 h, 12.3 g of NaCl were added and the final mixture was kept under stirring at 40℃ for m ore 22 h. Subsequently, the gel was aged at 100℃ during 3 days in a polypropylene bott le. The product was recovered by centrifugation, washed with distilled water until pH 6-7 and dried overnight at 80 ℃. The template was partially removed by extraction with 96% ethanol, at reflux temperature for 16h. The solid was further calcined under a flux of dry air (6L/g.h) at 550 ℃ for 12 h. The temperature was increased from 20 to 550 ℃ at 5 ℃/min.

The powder XRD pattern was recorded on a Panalytical X'Pert Pro diffractometer using CuKα radiation filtered by Ni and an X'Celerator detector. Nitrogen adsorption isotherm was measured at -196 ℃ using ASAP 2010 Micromeriti cs equipment. Prior to the measurement, the sample was degassed at 350 ℃ for 3 h.

SEM images were obtained on a JEOL JSM-7001F equipment coupled with an Oxford EDX detector and TEM images were obtained on a Hitachi H8100 equipment. Samples were deposited in a Cu/polymer grid sample holder.

Prior to use, SBA-15 was dried under a flux of dry air (4L/g.h) at 300 ℃ for 1 h. The temperature was increased from 20 to 300 ℃ at 5 ℃ /min. Then, the support was kept at this temperature during another 1 h under a nitrogen flow (4 L/g.h) and finally cooled to room temperature and stored under dry nitrogen in a Schlenk flask.

2.3 Ethylene polymerizations

Polymerizations were carried out in a 250 mL dried and nitrogen-flushed bottle for pressure reactions (Wilmad LabGlass LG-3921) magnetically stirred. The reactor was filled with 50 mL of toluene, the adequate amount of the co-catalyst MAO, the catalyst and ethylene. Polymerizations took place at 20 ℃ a nd 1.1 bar of ethylene. Temperature, pressure and ethylene consumption were monitored in real time and the data stored, enabling acquisition of kinetic profiles. The polymerization run until a given amount of ethylene was consumed allowing this way the preparation of HDPE nanocomposites with a given SBA-15 content. Polymerization mixtures were then quenched by the addition of methanol acidified with 5% HCl. The polymer was collected and washed twice with methanol before drying.

2.4 Preparation of the supported catalysts

Two different methods were used for the preparation of the supported catalysts as detailed below:

2.4.1 Pretreatment of SBA-15 with MAO and impregnation of the FI catalyst on pretreated support (Method SBA-MAO)

The SBA-15 was first treated with MAO in a Schlenk flask under nitrogen atmosphere at room temperature by addition of 1.75 mL of MAO to 1 g of support dispersed in 25 mL of toluene. After 16 h stirring, the solid is washed three times with ca. 20 mL of dry toluene and dried at room temperature under vacuum overnight. The aluminum load on

the support, determined by elemental analysis, is 2.7 mmol Al/g support. The distribution of Al from MAO in SBA-15 was assessed by Energy dispersive X-ray spectroscopy, by obtainment of Si and Al maps.

After drying, 100 mg of this MAO treated SBA-15 solid is contacted with 1.9 μmol of the FI catalyst in toluene (orange solution) and stirred for 4 min, complete discoloration of the toluene solution and transfer of color to the solid support was observed after this time, suggesting complete immobilization of the catalyst. Severn *et al.* also reported a transfer of color from the toluene solution to the solid support after complete immobilization of FI catalyst [28]. In order to confirm that all the FI catalyst is immobilized on the mesoporous solid, the catalyst suspension, obtained after 4 min of contact between the support and the catalyst solution, is allowed to decant. Then a small volume (~2 mL) of the clear supernatant liquid is tested in polymerization conditions, with further addition of MAO (same as used for polymerization runs). The polymerization test with this clarified solution does not exhibit any activity, confirming that no catalyst remained in the supernatant solvent [29]. Moreover elemental analysis of the supported catalysts showed the expected Ti content, corroborating the results of the clarified liquid test. Additional supported catalysts were prepared with higher impregnation times, in order to check the influence of this parameter on the polymerization activity.

2.4.2 Impregnation of MAO pre-activated FI catalyst on SBA-15 (Method PA)

The solution of FI catalyst in toluene is pre-activated with MAO (Al/Ti = 150) by stirring for 15 min at room temperature. After this time, the equivalent of 0.85 μmol of MAO pre-activated catalyst is mixed with 100 mg of the support in toluene and stirred for 90 min. As in method SBA-MAO, upon immobilization no activity of the supernatant liquid is shown in polymerization conditions, confirming that there is no catalyst remaining in homogeneous solution.

2.5 Characterization of the polymers

High temperature size exclusion chromatography (HT-SEC) analyses were performed using a Viscotek system (from Malvern Instruments) equipped with three columns (Polefin 300 mm x 8 mm I. D. from Polymer Standards Service, porosity of 1,000 Å, 100,000 Å and 1,000,000 Å). 200 µL of sample solutions with concentration of 5 $mg \cdot mL^{-1}$ were eluted in 1,2,4-trichlorobenzene using a flow rate of 1 $mL \cdot min^{-1}$ at 150 ℃. The mobile phase was stabilized with 2,6-di(*tert*-butyl)-4-methylphenol (200 $mg \cdot L^{-1}$). Online detection was performed with a differential refractive index detector and a dual light scattering detector (LALS and RALS) for absolute molar mass measurement. The OmniSEC 5.02 software was used for calculations.

Powders obtained after polymerization were processed as films by compression molding in a Collin P-200-P press between hot plates at 230 ℃ for 2.5 min without pressure, 3 min at a pressure of 5 bar, then 2 min at 10 bar. Cooling process was performed with cold water for 3 min at 10 bar.

Wide-angle X-ray diffraction (XRD) patterns were used for characterizing the crystalline features, these profiles being recorded at room temperature in the reflection mode by using a Bruker D8 Advance diffractometer provided with a PSD Vantec detector (from Bruker, Madison, Wisconsin). Cu Kα radiation (λ = 0.1542 nm) was used, operating at 40 kV and 40 mA. The parallel beam optics was adjusted by a parabolic Göbel mirror with horizontal grazing incidence Soller slit of 0.12° and LiF monochromator. The equipment was calibrated with different standards. A step scanning mode was employed for the detector. The diffraction scans were collected within the range of 2θ = 1–43°, with a 2 θ step of 0.024° and 0.2 s per step. Crystallinity a t room temperature was evaluated for the neat polyethylene samples by decomposition of the X-ray profile, after their normalization, into the different crystalline diffractions and the amorphous contribution. On the other hand, crystallinity estimation in the nanocomposites involves firstly subtracting the weight contribution of the SBA-15 amorphous halo at the angular range analyzed before deconvolution of the resulting patterns into the distinct polyethylene crystalline diffractions and amorphous contribution. The error in the crystallinity determinations is estimated to be ± 0.04.

Thermogravimetric analysis (TGA) was performed in a Q500 equipment of TA Instruments under air or nitrogen atmosphere at a heating rate of 10 ℃/min. Calorimetric analyses were carried out in a TA Instruments Q100 calorimeter connected to a cooling system and calibrated with different standards. The sample weights ranged from 3 to 5 mg. A temperature interval from -40 to 190 ℃ was studied at a heating rate of 10 ℃/min. For the determinati on of the crystallinity, a value of 290 J/g was used as the enthalpy of fusion of a perfectly crystalline material [30].

SEM and TEM micrographs were obtained as described above for the pure SBA-15. For the TEM analysis of PE nanocomposites films parallel cuts were prepared from different samples at -100ºC using a LEICA EM FC6 cryo-camera in order to attain thin sections (80nm) of the film surface by means of the LEICA EM UC6 ultramicrotome. Those cuts were picked up on cooper grids.

Depth Sensing Indentation, DSI, experiments were performed at room temperature with a Shimadzu tester (model DUH211S) equipped with a Berkovich type diamond indenter. In all specimens, at least 10 indentations were performed at different regions of surface. The experimental protocol consisted in: a) the application of a load of 10 mN at a loading speed of 1.46 mN/s; b) the maintenance of this constant load for 5 s, and c) the release of the load at an unloading speed equal than the one used along the loading stage. Finally, indentation depth was registered, additionally, for 5 s after reaching the minimum load (0.1 mN). Martens hardness, HMs, and indentation hardness, Hit, were calculated according to Oliver-Pharr method [31]. These two hardness values are given by the ratio of the maximum load to either the contact area under load or after releasing the indentor, respectively. Consequently, HMs is related to elastic, viscoelastic and permanent strains, whereas Hit only depends on viscoelastic and plastic strains.

The strain-stress tests were performed at two different temperatures, at 25 ℃ in an Instron 3366 dynamometer with a load of 100 N and at 90 ℃ in a Minimat 2000 dynamometer with a load of 20 N. Rate of uniaxial stretching was 1 mm/min at both

temperatures. Specimens for these experiments were punched out from the polymer films. The dimensions of these strips were 10 mm long, 2 mm wide and around 0.15 mm thick. All the samples were stretched until a final strain value of 350%.

3. Results and discussion

3.1 The support SBA-15

The powder XRD pattern of the as-synthesized SBA-15 (**Figure S1** of Supporting Information) shows the expected highly ordered two dimensional hexagonal structures, constituted by the arrays of uniform mesopores and identified by the three diffraction peaks that can be indexed as (100), (110) and (200) reflections associated with the *p6mm* hexagonal symmetry [32]. SEM and TEM micrographs of the SBA-15 synthesized are depicted in **Figure 1a** and **1b**, respectively, where the particle morphology and the well-defined channel structure with the hexagonal arrangement are evidenced.

Also in the Supporting Information, **Figure S2** displays the N_2 adsorption isotherm obtained for the sample of SBA-15 and **Table S1** summarizes the textural parameters calculated from this experimental isotherm, which are similar to others reported for this type of supports [33].

Moreover, SBA-15 exhibits an N_2 adsorption-desorption type IV isotherm with an H1 hysteresis, characteristic of well-formed SBA-15 material [33] with the presence of a well-defined pore filling step with a narrow range of p/p_0 (capillary condensation), demonstrating the fine organization of cylindrical pores of uniform size.

EDX maps of Al and Si were recorded in order to evaluate the MAO distribution on the surface of SBA-15 after modification and show a homogeneous distribution of Al on SBA-15 (**Figure S3** of Supporting Information). The retention of the ordered morphology after SBA-15 modification is also clearly seen by SEM.

3.2 Ethylene polymerization behavior of the homogeneous catalyst

FI catalysts combined with appropriate activators exhibit very high catalytic activity and particularly Ti-FI catalysts possessing fluorine atom(s) *ortho* to the imine-*N* can induce highly controlled living ethylene polymerizations [34, 35]. The bis [*N*-(3-tert-butylsalicylidene)-2,3,4,5,6-pentafluoroanilinate] titanium (IV) dichloride (represented in **Scheme 1**) was used as catalyst to produce UHMWPE under homogeneous conditions, as reported in former studies [36, 37].

The effect of experimental parameters, such as Al/Ti ratio and polymerization time, on the behavior of this complex under homogeneous conditions was first investigated. The obtained results are summarized in **Table 1** and **Figure S4** (in the Supporting Information).

Figure S4 shows the kinetic profiles obtained for several Al/Ti ratios at distinct polymerization times. It may be seen that quite stable profiles are obtained for polymerizations carried out for 6.5 min or 13 min but the activity decay is much more pronounced at longer polymerization runs. Accordingly, the average activity and productivity (see **Table 1**) show almost a two-fold increase when the polymerization time increases from 6.5 to 13 min, but this linear dependence is lost at the highest polymerization time of 26 min. The behavior exhibited at short reaction times is in accordance with the reported living character, whereas it starts to deviate from purely living characteristics as polymerization times become longer [38].

The analysis of the polymer molar masses shows however that the catalytic system is already deviating from a living character at low polymerization time, showing a polydispersity index, PDI, of 1.3, and this deviation is enlarged with time reaching a PDI of 1.6 after 26 min. Heterogenization of the catalyst and mass transport limitations within the growing polymer particles enclosing the active sites or a gradual deactivation of the catalyst by the growing polymer after a certain polymerization time have been proposed to account for this deviation [39, 40]. Accordingly and due to these phenomena, the dependence of the activity on the Al/Ti ratio only exhibits an

increasing trend for the runs at the shortest polymerization times. Although, data on the effect of Al/Ti over polymerization is scarce for this type of catalyst, a similar dependence has been described by other authors [41, 42]. On the other hand, a stronger decay of the instantaneous activity seems to occur at the highest Al/Ti ratios (Figure S4, right plot, in Supporting Information) therefore, the role that may play the increasing concentration of trimethylaluminum, invariably present in MAO, in deactivation of FI catalyst should not be neglected [43, 44].

Lemstra *et al.* reported that rising Al/Ti ratio results in an increase of the molar mass, arguing that the chain transfer to aluminum does not play a major role in their catalytic system [38]. In the present conditions, the values of M_w obtained for polymerizations at identical reaction time (6.5 min) FIHOM014, FIHOM008 and FIHOM005 indicate that molar mass barely increases with the Al/Ti ratio. This behavior may be explained by two different effects acting simultaneously: on one hand, the increase of the Al/Ti would promote the activation and stabilization of the catalytic species but, on the other hand, a detrimental influence is also expected with the rise of Al/Ti ratio due to the easy deactivation of the catalyst by the trimethylaluminum present in MAO. The balance of these two opposing effects will determine the catalytic behavior that, under the conditions here used, gives rise just to a slight increase in the polymer molar masses. On the contrary, at constant Al/Ti ratio an increase in the polymerization time significantly increases the polymer molar mass, as clearly deduced from Table 1. Nevertheless, the catalyst starts deviating from the living character at short polymerization times, as a non-linear M_n dependence on time is observed.

3.3 Ethylene polymerization behavior of the supported catalyst

Two different immobilization methods have been used in this work to perform the synthesis of UHMWPE nanocomposites by *in situ* supported polymerization. Methylaluminoxane (MAO) is needed in both for the FI catalyst to be immobilized on the SBA-15. The direct impregnation of FI catalyst on SBA-15 was also attempted in an

early stage but it was proved to be ineffective. In fact, to the best of our knowledge, there is no reported data in open literature regarding the direct immobilization of this catalyst on any type of silica. Steric reasons may account, most probably, for this feature.

The first approach used involves immobilization of the catalyst on SBA-15 formerly modified with MAO (SBA-MAO method), as displayed in **Scheme 2**. This is one of the most widely used techniques to support catalysts and comprises the treatment of the silica surface with MAO before incorporation of catalyst to form the catalytic complex with the surface-anchored MAO [45]. Other authors have used the same methodology to immobilize FI catalysts on silica. Cui *et al*. carried out ethylene polymerization with dried SiO_2 firstly treated with MAO and then with a titanium complex that turned out in polymers with a higher molar mass, a higher melting temperature and a better morphology than the ones obtained with the corresponding homogeneous catalyst [46]. Carlini *et al.* anchored a nickel catalyst to MAO-treated silica and obtained a thermally stable nickel-heterogenized catalyst able to polymerize ethylene with higher productivity in comparison with its homogeneous counterpart [47]. The same procedure was applied to mesoporous silicas: a zirconium FI complex was immobilized on SBA-15/MAO and nanofibrous polyethylene was produced [48]. Another zirconium-FI complex supported on MCM-41/MAO leaded to extended-chain polyethylene nanofibrils with diameters of about 10 – 100 nm [49].

The second method implies the pre-activation of catalyst with MAO prior to its contact with SBA-15 (PA method). This route was applied before to metallocene catalysts and it was reported that the number of active sites was increased, leading to highly active catalysts. This method has also the benefit of simplifying the experimental set-up for immobilization (see **Scheme 3**).

Both treatments were performed in a way that the final Al/Ti ratio is the same after the immobilization of the catalyst. The influence of these two routes on activity and polymer properties will be discussed now. Results listed in **Table 2** indicate a significant

decrease of the activity upon FI immobilization on SBA-MAO, as compared with those values shown in **Table 1** for neat polyethylenes achieved under homogeneous conditions. This is a common feature when catalysts are supported and it is generally attributed to catalyst deactivation pathways during immobilization. For the FI catalyst type, this aspect may be even more pronounced in the present conditions, since MAO has been used to immobilize the FI catalyst.

It is well known from literature that titanium FI-catalysts are very sensitive toward trimethylaluminum (TMA), which is always present in the co-catalyst MAO [43, 44]. The proposed deactivation pathway is depicted in **Scheme 4** [35]. In the presence of TMA, one of the ligands is abstracted from the cationic Ti species **2** with the consequent formation of the species **3**. The resulting Al and Ti species are barely active for olefin polymerization. Indeed, in the case of ethylene polymerization promoted by the homogeneous FI catalyst it was observed a decrease of the activity of ca. 30% (from 20380 to 13870 kgPE/mol Ti.h) when using a pre-activated catalyst (which was contacted during 15 min with MAO prior to polymerization) while maintaining the other experimental conditions identical to those used for the FIHOM008 homopolymer.

The pre-treatment of the SBA-15 with MAO is expected to generate surface-bonded Si-O-Al$(Me)_2$ species [50] that may be involved as well in ligand transfer reactions and even enhance them relatively to those occurring with free TMA. Therefore, higher catalyst deactivation may be expected for the supported catalysts.

In relation to this reasoning, the polymerization activity is significantly reduced by increasing the time of contact between the FI catalyst and the SBA-MAO support (from 4 to 180 min), as observed when comparing the samples FISBA007, FISBA004 and FISBA003. It is also worthwhile to notice that a significant decrease of the molar masses and a broadening of the molar mass distribution are revealed when applying the SBA-MAO method for the immobilization of FI catalyst). This observation corroborates our assumption related to the significant enhancement under these conditions of the deactivation pathways inhibiting living propagation.

In the PA approach, the FI catalyst is pre-activated by the addition of MAO in a ratio of Al to Ti of 150:1 for 15 min, and then the FI-MAO system is contacted with the SBA support. During pre-activation, the orange catalyst turned brownish, which may indicate that certain amount of the catalyst could be decomposed, a fact that might contribute to the decrease in the polymerization activity observed. This is in agreement with the already mentioned decomposition of titanium FI catalyst by the presence of TMA [43]. An interesting feature is that by using the PA method the time necessary for immobilization significantly increases in relation to the previous method. Despite the longer impregnation time that is expected to promote the detrimental effect of TMA over FI catalyst, higher activities are surprisingly obtained. In this case, a fraction of the catalyst is deactivated during the catalyst pre-activation by action of free TMA, but the support has not been previously pre-treated with MAO and, accordingly, a lower amount of surface-bonded Si-O-Al$(Me)_2$ species are expected. Therefore, the deactivation pathways that may involve these surface-bonded species are reduced. Consequently, at similar experimental conditions, the polymer molar mass obtained with the PA method is considerably higher than that achieved using SBA-MAO route. As a general trend the nanocomposites, independently of the immobilization method used for its synthesis, show a broadening of the molar mass distribution when compared to the values obtained for the neat polyethylene samples.

In order to determine if significant diffusional aspects may be operating, the normalized kinetic profiles of representative homogeneous and supported catalytic systems are shown in **Figure 2.**

It can be seen that all the curves exhibit a fast increase of the initial activity as well as short and similar induction periods, characteristic of the catalytic systems without significant diffusional constraints. It is worthwhile to notice that the homogeneous and the PA systems show analogous deactivation trends, while a slightly higher deactivation rate is observed for the SBA-MAO method. This may be related to the

presence of higher amounts of the surface-bonded Si-O-Al(Me)$_2$ species, as already mentioned.

Figure 3 shows the morphology found by SEM in powder samples, obtained directly from the reactor, for a neat polyethylene and two nanocomposites synthesized under the two distinct immobilization approaches. The formation of fibrils in the composites is well evident, while in the neat polyethylene these elongated fibrils are hardly observed. Moreover, it seems that the latter are more numerous and narrower in FISBA017 than in FISBA007 sample.

3.4 Characterization of the polyethylene based materials

3.4.1 Evidence of SBA-15 on the nanocomposites

SBA-15 used as catalyst support for the synthesis of polyethylene was not removed at the end of polymerization stage. As the polymerization is expected to occur both in the external surface and within the mesoporous, the resulting materials can be considered nanocomposites comprising a polymeric matrix and the mesoporous SBA-15 particles as filler. XRD profiles do not provide information concerning the spatial distribution of the mesoporous material within the polymer matrix but it allows assessing the presence of SBA-15 in the final nanocomposite. **Figure S5** in Supporting Information shows the X-ray pattern of SBA-15, a polyethylene homopolymer and a nanocomposite at the low angle region. The polyethylene (sample FIHOM014) does not show any diffraction peak at that low angle region ($2\theta < 5^\circ$). The presence of diffraction peaks in this region for the nanocomposites samples clearly indicates that SBA-15 retains its structural integrity during the polymerization process. This is corroborated by the TEM micrograph of FISBA017 sample at high magnification, where the regular pore structure of SBA-15 is clearly seen (see **Figure S6** in Supporting Information).

3.4.2 Thermogravimetric analysis

Once different UHMWPE based materials, either neat polyethylenes or those incorporating SBA-15, have been synthesized through different methodologies,

knowledge of some of their physical characteristics is required. The choice of the specimens to be characterized has been mainly made depending on the amount of UHMWPE based material produced and the amount required for a given experiment. Thermogravimetry allows learning about the thermal stability exhibited by specimens, the distinct decomposition processes involved depending on the atmosphere used and, the determination of the SBA-15 amount in the nanocomposites. It has been observed that the content estimated at a given specimen is rather independent of the environment used, mainly in those nanocomposites prepared by the approach where FI catalyst has been pre-activated with MAO before the further impregnation on SBA-15 surface, labeled as PA. Average values obtained from inert and oxidative conditions are listed in **Table 3**.

Figure 4 shows the thermogravimetry curves under inert and air environments for some of the different polymeric materials. Under inert conditions, a single primary stage of decomposition is observed in the temperature range from 200 to 650 ℃ for the pristine UHMWPE and the different composites, as represented in the upper plots on the left and right, respectively. Thermal decomposition of polyethylene has been reported to occur under these conditions through a random scission mechanism that turns out in the rupture of original polymeric chain into fragments of varying length. The mechanism describes a random generation of free radicals along the polymer backbone, followed by the scission of the chain that results in the formation of a molecule with an unsaturated end and another with a terminal free radical. Subsequent hydrogen chain transfer reactions transform the radical fragments into straight chain dienes, alkenes and alkanes [51].

Four different degradation processes are, however, noticeable at identical temperature interval when air is the environment used, as depicted in the bottom plots of **Figure 4**. It is well known that the initial reaction of the polyethylene thermal oxidation is the formation of alkyl radicals from polymeric chains followed by the reaction of alkyl radicals with oxygen to form hydroperoxides, which can decompose to alkoxyl radicals.

Then, the alkoxyl radicals abstract hydrogen from the chain and other alkyl radical forms. Finally, various carbonyl species are generated.

Molar mass seems not to affect much the temperature at which decomposition reaches a 25 % loss of weight in the neat UHMWPE. However, it is clearly noticeable in **Figure 4** that presence of SBA-15 alters the thermal stability in the hybrids when compared with that presented by the neat UHMWPEs under inert conditions. The temperature at which the mass loss is 25 wt. % is shifted to lower values in the hybrids (with the exception of FISBA016 that presents the highest $M_{w,}$ around 2 millions) in comparison with those found in the neat UHMWPE although decomposition process starts at similar temperatures.

Moreover, it seems that the synthetic approach is important for the decomposition characteristics exhibited under oxidative conditions. In fact, the 5 % weight loss occurs at temperatures slightly higher in the SBA_MAO materials compared with the PA ones while still higher differences are found for $T_{25\%}$. These features point out a catalytic outcome of the presence of small amounts of SBA-15 in these PA samples. In fact, MCM-41, which is other mesostructured silica particle, is frequently used as degradation catalyst. An important shift to lower temperatures of the main degradation process under inert conditions has been reported with increasing MCM-41 composition [21] in nanocomposites prepared by *in situ* polymerization of mesoporous MCM-41 and ethylene, the former also acting as catalyst carrier and as nanofiller. The catalytic degradation mechanism implies an initial cracking of large hydrocarbon molecules into small C3–C5 olefins in the catalytically active sites, followed by oligomerization, cyclization and hydrogen transfer reactions that result in the formation of aromatics, light paraffins and olefins.

3.4.3 Differential Scanning Calorimetry (DSC)

The DSC results are summarized in **Table 4** and **Figure 5. Table 4** reports information on the first melting process of samples obtained either from the reaction powder or the corresponding processed films. As a general trend, independently of being synthesized

under homogeneous or supported conditions, there is a significant difference in crystallinity and melting temperature between both types of specimens: reactor powders and films. Crystallinity and melting temperature, this last one directly related to the size of crystalline entities, are considerable larger in the as-powder samples, because disentangled chains are able to crystallize during polymerization giving rise to rather chain-extended crystals with a very small proportion of amorphous regions. On the contrary, chains after melting, because of their large length and the high mobility degree that they possess at those high temperatures, are able to establish a great number of entanglements between them and crystal formation will be hindered during crystallization along the cooling process applied for films manufacture. Then, a significant reduction is observed in crystallinity and melting temperature of the crystallites generated during film processing.

Moreover, results point out that the different homogeneous UHMWPE samples exhibit crystallinity values slightly higher than those in the supported specimens that incorporate SBA-15 (with the exception of FISBA004 that shows an analogous value in the as-powder sample and the highest one in the film,). This feature is a general trend since this lower crystallinity is evident in the as-powder sample as well as during first melting of films and their further crystallization. In addition, presence of SBA-15 particles slightly inhibits UHMWPE crystallization. Nevertheless, transition temperatures (melting temperatures and crystallization temperatures) are not strongly affected by the SBA-15 presence.

The trend in crystallinity values has been confirmed by their determination from X-ray measurements at room temperature. The crystallinity degrees obtained have been also included in Table 4 and the corresponding profiles can be seen in **Figure S7** of Supporting Information. It is found that the neat polyethylene samples show crystallinities slightly higher than those exhibited by the nanocomposites, this fact corroborating the DSC results.

Figure 5b shows that there are some differences in the thermal behavior of the nanocomposites, at temperature ranging from 80 to 110 ℃, depending on the synthetic approach used. At that interval, a small shoulder is observed in the specimens prepared by PA method while its presence is rather less evident in those SBA-MAO samples. That small endothermic peak is attributed to those UHMWPE crystallites that are developed inside the SBA-15 channels, similarly to evidences found in nanocomposites with MCM-41 [21]. Channel confinement prevents a further growth of the crystallites and, accordingly, these crystalline entities generated within SBA-15 particles are of much smaller size than those that can grow at its surface and in the UHMWPE bulk. Then, melting temperature is much lower. Therefore, this feature seems to point out that there are none or a very small amount of crystallites within SBA-15 channels in samples synthesized by SBA-MAO approach. This may also be in relation to the earlier decomposition of samples obtained by PA method (where UHMWPE crystallites are developed inside the SBA-15 channels) compared to SBA-MAO and UHMWPE samples.

3.4.4 Stress-strain behaviour

Left plot of **Figure 6** depicts the stress-strain behavior at room temperature for two homopolymers, FIHOM004 and FIHOM002, and their comparison with two nanocomposites, FISBA004 and FISBA016 representative of the two immobilization methodologies used. **Table 5** lists the different parameters obtained for the several samples at the two temperatures analyzed. The stress-strain curves for all these specimens are characteristic for ductile polymers. Results demonstrate that there are practically no differences between the two homopolymers neither in their mechanical parameters values nor in the whole deformation process, including cold drawing and strain hardening. These features are related to the similar molar mass of both UHMWPEs and, consequently, to analogous characteristics of their macromolecule entanglements, involving consequently, similar tensile strength and toughness.

The incorporation of SBA-15 particles leads, however, to stiffer materials with higher mechanical strength and toughness compared with those found in the neat homopolymers. Thus, the Young`s modulus, the σ_{end} and the value of the area under stress-strain curve are higher in FISBA004 and FISBA016 than in homopolymers FIHOM002 and FIHOM004. All these features are clearly deduced from the left plot of **Figure 6**. The best response is exhibited along the whole stress-strain curve for the FISBA016 nanocomposite. Therefore, it shows the higher mechanical parameters (E, σ_Y, σ_{end}), these features being associated with its superior SBA-15 content and much higher molar mass.

On the other hand, these two nanocomposites (FISBA004 and FISBA016) were prepared using two different methodologies. A straightforward correlation between the mechanical responses and the preparation approach cannot be undoubtedly established because, first of all, the final SBA-15 content is not identical in both of them. Secondly, analogous polymer-filler interactions are expected to be developed within these hybrids. Then, it seems that the most important factors that trigger deformation process in these nanocomposites are either the SBA-15 amount or further molar mass variations. The synthetic methodology may however play an indirect role as it might be responsible for obtaining materials with lower (those by SBA-MAO method) or higher (those by PA approach) molar masses or with a bigger or smaller proportion of PE chains within SBA-15 channels. Consequently, the FISBA016 hybrid exhibits the highest mechanical parameters (Young´s modulus, yield stress and tensile strength -as deduced from stress at the end of the experiment) compared with those shown by the homopolymers and by the other FISBA004 nanocomposite, which incorporates less SBA-15 amount and has lower M_w. Moreover, deformation process undergoes some changes from homopolymers to FISBA016 hybrid. Three stages are observed in the two homopolymers and the FISBA004: the initial elastic zone, a uniform region of cold-drawing and, finally, the strain hardening, which is more pronounced in the FISBA004 nanocomposite because of SBA-15 incorporation. Cold-

drawing stage is very narrow in the FISBA016 and, then, strain hardening starts at much lower strains because of its high rigidity and extremely high M_w. This superior stiffness and chain length will impose higher constraints for disentangling UHMWPE macrochains in the FISBA016 and, then, tensile strength increases compared with that found in the FISBA004 nanocomposite.

The effect of temperature is clearly deduced from the right plot in **Figure 6** and results listed in **Table 5**. All of mechanical parameters (Young´s modulus, yield stress and tensile strength) are significantly reduced with respect to those obtained at a given specimen at 25 ℃. Incorporation of SBA-15 particle s in the nanocomposite leads again to a stiffer material with high toughness. Differences in the mechanical parameters between the homopolymer and the nanocomposite are now more noticeable at this high temperature.

3.4.5 Indentation experiments

Indentation has been used as a fast and reliable mechanical test for the evaluation of the hardness, modulus and creep variations upon incorporation of the filler [52], in a way to get information on the rigidity and resistance of the materials to plastic deformation. The indentation results are depicted in **Figure 7** for loading-maintenance-unloading experiments performed in some of the homopolymers (left plot) and hybrids (right representation) under study. Significant variations are observed depending on the homopolymers molar mass and SBA-15 presence in the composites, both on the shape of curves and on the indentation depth reached. The FIHOM007 is the homopolymer with the highest M_w and, consequently, higher amount of entanglements; and the indenter cannot penetrate too much in its surface. The other two homopolymers, FIHOM004 and FIHOM002, exhibit a rather analogous M_w and indenter depth reached at identical load is larger, because both are softer than FIHOM007. Therefore, it seems that higher molar mass hinders indenter penetration under neat UHMWPE surface. Hardness is in agreement with this penetration hindrance and

values are very similar for FIHOM004 and FIHOM002 and lower than that found in FIHOM007.

Right plot in **Figure 7** proves the great influence that incorporation of SBA-15 particles exerts on these loading-maintenance-unloading processes. It is clearly seen that indenter can go more deeply into the material and, accordingly, depth attained is significantly enlarged in the FIHOM002 homopolymer compared with those achieved in the composites. Thus, SBA-15 acts as reinforcing agent and stiffer component and its content is in FISBA017 higher than in FISBA016. Nevertheless, M_w is just the opposite: in FISBA016 higher than in FISBA017. Results seem to indicate that for this mechanical measurement at composite surface the SBA-15 content is more crucial than a larger amount of entanglements. Consequently, depth reached at a given load is reduced in the FISBA017 nanocomposite, which contains the highest SBA-15 composition, and hardness value is enlarged.

Additional information can be deduced from the depth vs. indentation time representation, as displayed in **Figure 8**. The loading-maintenance-unloading processes are clearly observed as well as their dependence on molar mass and SBA-15 content. Thus, deformability is reduced and, accordingly, depth is decreased along loading stage if molar mass is increased in the homopolymers (upper plot) and if SBA-15 is incorporated. The maintenance at a constant load for 5 second allows learning on creep response of these materials. An increment of penetration depth is seen for all the specimens during this maximum load at 10 mN, L^{max}, i.e., during the maintenance period (see both plots in **Figure 8**). This depth is dependent again on molar mass and presence of SBA-15 in the ultimate material. Accordingly, homopolymers become more compliant as molar mass is lowered and their creep resistance is lower compared with that exhibited by the hybrids.

Figure 8 also displays that the unloading process is mainly dominated by the viscoelastic recovery of the different materials. Once experiment is over, a permanent deformation (plus a small amount of delayed elastic recovery) is attained in all the

specimens since they are not completely elastic. The softening process involves a very small rise of the amount in the plastic deformation in the samples with lowest molar masses. Moreover, a decrease in this viscous and non-reversible contribution is observed as SBA-15 content is raised.

Properties in nanocomposites are usually highly dependent on minor component content and also on its distribution [53]. **Figure S8** of supporting information shows the SEM images of the UHMWPE/SBA-15 materials and it allows learning about particle distribution and size of the agglomerates of the SBA-15 within the polyethylene matrix. SBA-15 is not uniformly dispersed within the UHMWPE matrix. Thus, the resulting nanocomposite turns out heterogeneous. The maximum SBA-15 content tested in the present work is 8.5 wt. % due to the known tendency of silica to agglomerate. Nanofiller loadings higher than 10 wt. % are frequently not considered because agglomeration starts to play a significant role and mechanical enhancement levels-off or even decreases. A 10% E increase was found upon addition of 5.0 wt.% raw MWCNTs to UHMWPE [54], ascribed to the poor nanofiller-matrix interface, the presence of voids and the nanotube waviness that limits the efficiency of the reinforcement. **Figure S9** shows the TEM micrographs of two nanocomposites, FISBA007 and FISBA016, representative of each immobilization method used. No significant changes on overall morphology can be detected.

4. Conclusions

Different UHMWPE homopolymers have been synthesized using a FI catalyst with living character. Moreover, this catalyst has been immobilized by two different approaches onto SBA-15 particles giving rise to UHMWPE based composites.

Very high activities in ethylene polymerization are obtained for the homogeneous FI catalyst, as expected from literature data. Moreover, the average activity and the productivity display almost a linear increase at those low times, although this linearity is lost at highest times. Dependence of molar masses on polymerization time shows

deviations from that expected living character even at low times in the polyethylenes prepared with the homogeneous catalyst. On the other hand, an increase in Al/Ti ratio seems not to affect significantly molar masses in the UHMWPE homopolymers. This behavior might be explained by the balance of two opposite effects acting simultaneously: promotion of the activation and stabilization of catalytic species and a detrimental deactivation of the catalyst by the presence of trimethylaluminum, TMA, in methylaluminoxane.

An important decrease of the activity is observed upon immobilization of the FI catalyst by the SBA-MAO methodology. This reduction is more considerable than that undergone when FI catalyst is supported by the pre-activated approach in spite of the shorter impregnation time required by the former method. It is suggested that the deactivation pathways that may involve Si-O-Al$(Me)_2$ surface-bonded species are lowered using the latest methodology.

Decomposition characteristics exhibited under oxidative conditions seem to be affected by the synthetic approach used during preparation of UHMWPE/SBA-15 materials. Nevertheless, none specific trend is seen under inert environment.

Very high crystallinity values are exhibited by the distinct UHMWPE samples in the form of as-powder from the reactor, either homopolymers or composites, in comparison with those estimated from films. Moreover, crystallinity from the first melting process is in the homopolymers generally higher than that in the hybrid materials independently of the approach used for their preparation. Nevertheless, transition temperatures (melting temperatures and crystallization temperatures) are rather independent of the SBA-15 presence and of the method for supporting the FI catalyst. On the other hand, composite specimens prepared by PA show a weak but noticeable shoulder on heating from 80 to 110 ℃, which is attributed to the melti ng of those UHMWPE crystallites developed inside the SBA-15 channels.

The incorporation of SBA-15 particles leads to stiffer materials, as deduced from stress-strain and indentation measurements, with higher elastic modulus, mechanical

strength and toughness compared with those magnitudes found in the neat homopolymers. Moreover, it seems that the most important factor that triggers deformation process is, in these nanocomposites, the SBA-15 amount followed by molar mass variations. Homopolymers become more compliant as molar mass is diminished and their creep resistance is lower compared with that exhibited by the hybrids.

Acknowledgments

Financial support of Fundação para a Ciência e Tecnologia, Portugal (SFRH/BD/72761/2010 and UID/QUI/00100/2013), PAUILF (Project TC 07/13) and of MINECO-Spain (Projects MAT2013-47972-C2-1-P and MAT2013-47972-C2-2-P) is acknowledged. The authors thank Dr. Enrique Vallés (PLAPIQUI - CONICET, Argentina) for support within GPC analysis.

5. References

[1] G. Wypych, UHMWPE ultrahigh molecular weight polyethylene, in: G. Wypych (Ed.) Handbook of Polymers, Elsevier, Oxford, 2012, pp. 672-676.
[2] S. Spiegelberg, Chapter 24 - Characterization of Physical, Chemical, and Mechanical Properties of UHMWPE, in: S.M. Kurtz (Ed.) UHMWPE Biomaterials Handbook (Second Edition), Academic Press, Boston, 2009, pp. 355-368.
[3] S.M. Kurtz, Chapter 1 - A Primer on UHMWPE, in: S.M. Kurtz (Ed.) UHMWPE Biomaterials Handbook (Second Edition), Academic Press, Boston, 2009, pp. 1-6.
[4] K.S. Katti, Biomaterials in total joint replacement, Colloids and Surfaces B: Biointerfaces, 39 (2004) 133-142.
[5] A. Ianuzzi, C. Mkandawire, Chapter 11 - Applications of UHMWPE in Total Ankle Replacements, in: S.M. Kurtz (Ed.) UHMWPE Biomaterials Handbook (Second Edition), Academic Press, Boston, 2009, pp. 153-169.
[6] V.A. Beloshenko, A.V. Voznyak, Y. V. Voznyak, G.V. Dudarenko, Equal-channel multiple angular extrusion of polyethylene, Journal of Applied Polymer Science, 127 (2013) 1377-1386.
[7] J. Cybo, J. Maszybrocka, P. Duda, Z. Bartczak, A. Barylski, S. Kaptacz, Properties of ultra-high-molecular-weight polyethylene with a structure modified by plastic deformation and electron-beam irradiation, Journal of Applied Polymer Science, 125 (2012) 4197-4208.
[8] B.M. Amoli, S.A.A. Ramazani, H. Izadi, Preparation of ultrahigh-molecular-weight polyethylene/carbon nanotube nanocomposites with a Ziegler–Natta catalytic system and investigation of their thermal and mechanical properties, Journal of Applied Polymer Science, 125 (2012) E453-E461.
[9] Y. Sánchez, C. Albano, A. Karam, R. Perera, E. Casas, In situ Polymerization of Nanocomposites by $TpTiCl_2(Et)$ System: UHMWPE Filled with Carbon Nanotubes, Macromolecular Symposia, 282 (2009) 185-191.
[10] X. Dangsheng, Friction and wear properties of UHMWPE composites reinforced with carbon fiber, Materials Letters, 59 (2005) 175-179.

[11] M. Deng, S.W. Shalaby, Properties of self-reinforced ultra-high-molecular-weight polyethylene composites, Biomaterials, 18 (1997) 645-655.
[12] S.C. Tjong, Structural and mechanical properties of polymer nanocomposites, Materials Science and Engineering: R: Reports, 53 (2006) 73-197.
[13] A. Dorigato, Y. Dzenis, A. Pegoretti, Filler aggregation as a reinforcement mechanism in polymer nanocomposites, Mechanics of Materials, 61 (2013) 79-90.
[14] M.Q. Zhang, M.Z. Rong, H.B. Zhang, K. Friedrich, Mechanical properties of low nano-silica filled high density polyethylene composites, Polymer Engineering & Science, 43 (2003) 490-500.
[15] D. Olmos, F. Martínez, G. González-Gaitano, J. González-Benito, Effect of the presence of silica nanoparticles in the coefficient of thermal expansion of LDPE, European Polymer Journal, 47 (2011) 1495-1502.
[16] W. Kaminsky, A. Funck, K. Wiemann, Nanocomposites by In Situ Polymerization of Olefins with Metallocene Catalysts, Macromolecular Symposia, 239 (2006) 1-6.
[17] S. Park, I.S. Choi, Production of Ultrahigh-Molecular-Weight Polyethylene/Pristine MWCNT Composites by Half-Titanocene Catalysts, Advanced Materials, 21 (2009) 902-905.
[18] C.T. Kresge, M.E. Leonowicz, W.J. Roth, J.C. Vartuli, J.S. Beck, Ordered mesoporous molecular sieves synthesized by a liquid-crystal template mechanism, Nature, 359 (1992) 710-712.
[19] J.S. Beck, J.C. Vartuli, W.J. Roth, M.E. Leonowicz, C.T. Kresge, K.D. Schmitt, C.T.W. Chu, D.H. Olson, E.W. Sheppard, A new family of mesoporous molecular sieves prepared with liquid crystal templates, Journal of the American Chemical Society, 114 (1992) 10834-10843.
[20] J.M. Campos, J.P. Lourenço, H. Cramail, M.R. Ribeiro, Nanostructured silica materials in olefin polymerisation: From catalytic behaviour to polymer characteristics, Progress in Polymer Science, 37 (2012) 1764-1804.
[21] M.L. Cerrada, E. Pérez, J.P. Lourenço, J.M. Campos, M. Rosário Ribeiro, Hybrid HDPE/MCM-41 nanocomposites: Crystalline structure and viscoelastic behaviour, Microporous and Mesoporous Materials, 130 (2010) 215-223.
[22] A. Kurek, S. Mark, M. Enders, M.O. Kristen, R. Mülhaupt, Mesoporous Silica Supported Multiple Single-Site Catalysts and Polyethylene Reactor Blends with Tailor-Made Trimodal and Ultra-Broad Molecular Weight Distributions, Macromolecular Rapid Communications, 31 (2010) 1359-1363.
[23] X. Dong, L. Wang, G. Jiang, Z. Zhao, T. Sun, H. Yu, W. Wang, MCM-41 and SBA-15 supported Cp_2ZrCl_2 catalysts for the preparation of nano-polyethylene fibres via in situ ethylene extrusion polymerization, Journal of Molecular Catalysis A: Chemical, 240 (2005) 239-244.
[24] G.C. Xu, A.Y. Li, L. De Zhang, X.Y. Yu, T. Xie, G.S. Wu, Nanomechanic Properties of Polymer-Based Nanocomposites with Nanosilica by Nanoindentation, Journal of Reinforced Plastics and Composites, 23 (2004) 1365-1372.
[25] J.M. Campos, J.P. Lourenço, E. Pérez, M.L. Cerrada, M.R. Ribeiro, Self-Reinforced Hybrid Polyethylene/MCM-41 Nanocomposites: *In-Situ* Polymerisation and Effect of MCM-41 Content on Rigidity, Journal of Nanoscience and Nanotechnology, 9 (2009) 3966-3974.
[26] M.L. Cerrada, E. Pérez, J.P. Lourenço, A. Bento, M.R. Ribeiro, Decorated MCM-41/polyethylene hybrids: Crystalline details and viscoelastic behavior, Polymer, 54 (2013) 2611-2620.
[27] A. Bento, J.P. Lourenço, A. Fernandes, M.L. Cerrada, M. Rosário Ribeiro, Functionalization of Mesoporous MCM-41 (Nano)particles: Preparation Methodologies, Role on Catalytic Features, and Dispersion Within Polyethylene Nanocomposites, ChemCatChem, 5 (2013) 966-976.
[28] J.R. Severn, J.C. Chadwick, Activation of Titanium-Based Single-Site Catalysts for Ethylene Polymerization Using Supports of Type $MgCl_2/AlR_n(OEt)_{3-n}$, Macromol. Chem. Phys., 205 (2004) 1987-1994.

[29] J.M. Campos, M.R. Ribeiro, J.P. Lourenço, A. Fernandes, Ethylene polymerisation with zirconocene supported in Al-modified MCM-41: Catalytic behaviour and polymer properties, Journal of Molecular Catalysis A: Chemical, 277 (2007) 93-101.
[30] F.A. Quinn, L. Mandelkern, Thermodynamics of Crystallization in High Polymers: Poly-(ethylene)1, J. Am. Chem. Soc., 80 (1958) 3178-3182.
[31] W.C. Oliver, G.M. Pharr, An improved technique for determining hardness and elastic modulus using load and displacement sensing indentation experiments, J. Mater. Res., 7 (1992) 1564-1583.
[32] D. Zhao, Q. Huo, J. Feng, B.F. Chmelka, G.D. Stucky, Nonionic Triblock and Star Diblock Copolymer and Oligomeric Surfactant Syntheses of Highly Ordered, Hydrothermally Stable, Mesoporous Silica Structures, J. Am. Chem. Soc., 120 (1998) 6024-6036.
[33] T. Klimova, A. Esquivel, J. Reyes, M. Rubio, X. Bokhimi, J. Aracil, Factorial design for the evaluation of the influence of synthesis parameters upon the textural and structural properties of SBA-15 ordered materials, Microporous Mesoporous Mat., 93 (2006) 331-343.
[34] M.C. Baier, M.A. Zuideveld, S. Mecking, Post-Metallocenes in the Industrial Production of Polyolefins, Angew. Chem. Int. Ed., 53 (2014) 9722-9744.
[35] H. Makio, H. Terao, A. Iwashita, T. Fujita, FI Catalysts for Olefin Polymerization—A Comprehensive Treatment, Chemical Reviews, 111 (2011) 2363-2449.
[36] M. Mitani, J.-i. Mohri, Y. Yoshida, J. Saito, S. Ishii, K. Tsuru, S. Matsui, R. Furuyama, T. Nakano, H. Tanaka, S.-i. Kojoh, T. Matsugi, N. Kashiwa, T. Fujita, Living Polymerization of Ethylene Catalyzed by Titanium Complexes Having Fluorine-Containing Phenoxy−Imine Chelate Ligands, Journal of the American Chemical Society, 124 (2002) 3327-3336.
[37] A. Iwashita, M.C.W. Chan, H. Makio, T. Fujita, Attractive interactions in olefin polymerization mediated by post-metallocene catalysts with fluorine-containing ancillary ligands, Catal. Sci. Technol., 4 (2014) 599-610.
[38] S. Talebi, R. Duchateau, S. Rastogi, J. Kaschta, G.W.M. Peters, P.J. Lemstra, Molar Mass and Molecular Weight Distribution Determination Of UHMWPE Synthesized Using a Living Homogeneous Catalyst, Macromolecules, 43 (2010) 2780-2788.
[39] S.S. Ivanchev, V.K. Badaev, N.I. Ivancheva, S.Y. Khaikin, Living Polymerization of Ethylene on the Bis[N-(3-tert-butylsalicylidene)anilinato]titanium Dichloride–Methylalumoxane Catalyst System, Doklady Phys. Chem., 394 (2004) 46-49.
[40] S. Ivanchev, V. Trunov, V. Rybakov, D. Al'bov, D. Rogozin, Structure and Catalytic Activity of Titanium and Zirconium Phenoxyimine Complexes, Doklady Phys. Chem., 404 (2005) 165-168.
[41] G. Zohuri, S. Damavandi, S. Ahmadjo, R. sandaroos, M. Shamekhi, Synthesis of high molecular weight polyethylene using FI catalyst, Polyolefins J., 1 (2014) 25-32.
[42] R. Sandaroos, S. Damavandi, A. Farhadipour, A New Family of High-Performance Ti Catalysts for Olefin Polymerization, Macromol. Chem. Phys., 211 (2010) 2339-2346.
[43] H. Makio, T. Fujita, Observation and identification of the catalytically active species of bis(phenoxy-imine) group 4 transition metal complexes for olefin polymerization using 1H NMR spectroscopy, Macromolecular Symposia, 213 (2004) 221-234.
[44] K.P. Bryliakov, E.A. Kravtsov, D.A. Pennington, S.J. Lancaster, M. Bochmann, H.H. Brintzinger, E.P. Talsi, Active Intermediates in Ethylene Polymerization over Titanium Bis(phenoxyimine) Catalysts, Organometallics, 24 (2005) 5660-5664.
[45] M.R. Ribeiro, A. Deffieux, M.F. Portela, Supported Metallocene Complexes for Ethylene and Propylene Polymerizations: Preparation and Activity, Industrial & Engineering Chemistry Research, 36 (1997) 1224-1237.
[46] K. Cui, B. Liu, C. Wang, J.-Y. Yu, Z. Ma, A silica-supported titanium(IV) complex bearing [O−NS] tridentate ligand and its behavior in ethylene homo- and copolymerization with 1-hexene, Journal of Molecular Catalysis A: Chemical, 266 (2007) 93-99.

[47] C. Carlini, A. Ceccarini, E.G. Fernandes, A.M.R. Galletti, G. Sbrana, Ethylene polymerization with silica-supported bis[3,5-dinitro-N-(2,6-diisopropylphenyl) salicylaldiminate]nickel(II)/methylaluminoxane catalysts, Journal of Polymer Science Part A: Polymer Chemistry, 43 (2005) 1978-1984.
[48] C. Guo, D. Zhang, F. Wang, G.-X. Jin, Nanofibers of polyethylene produced by SBA-15 supported zirconium catalyst [N-(3-tert-butylsalicylidene)-4-allyloxylanilinato]$_2$Zr(IV)Cl2, J. Catal., 234 (2005) 356-363.
[49] S. Chen, C. Guo, L. Liu, H. Xu, J. Dong, Y. Hu, Immobilization of a zirconium complex bearing bis(phenoxyketimine) ligand on MCM-41 for ethylene polymerization, Polymer, 46 (2005) 11093-11098.
[50] V.N. Panchenko, N.V. Semikolenova, I.G. Danilova, E.A. Paukshtis, V.A. Zakharov, IRS study of ethylene polymerization catalyst SiO_2/methylaluminoxane/zirconocene, J. Mol. Catal. A: Chem., 142 (1999) 27-37.
[51] F.S.M. Sinfrônio, A.G. Souza, I.G. Santos, V.J. Fernandes Jr, C. Novák, Z. Éhen, Influence of H-ZSM-5, Al-MCM-41 and acid hybrid ZSM-5/MCM-41 on polyethylene decomposition, J Therm Anal Calorim, 85 (2006) 391-399.
[52] A.M. Díez-Pascual, M.A. Gómez-Fatou, F. Ania, A. Flores, Nanoindentation in polymer nanocomposites, Prog. Mater Sci., 67 (2015) 1-94.
[53] J.K. Adewole, U.A. Al-Mubaiyedh, A. Ul-Hamid, A.A. Al-Juhani, I.A. Hussein, Bulk and surface mechanical properties of clay modified HDPE used in liner applications, The Canadian J. of Chem. Eng., 90 (2012) 1066-1078.
[54] S.R. Bakshi, K. Balani, T. Laha, J. Tercero, A. Agarwal, The nanomechanical and nanoscratch properties of MWNT-reinforced ultrahigh-molecular-weight polyethylene coatings, JOM, 59 (2007) 50-53.

Scheme 1

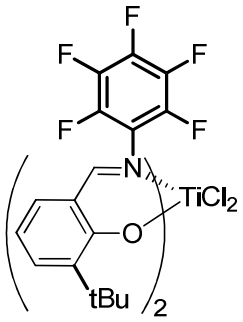

Scheme 2

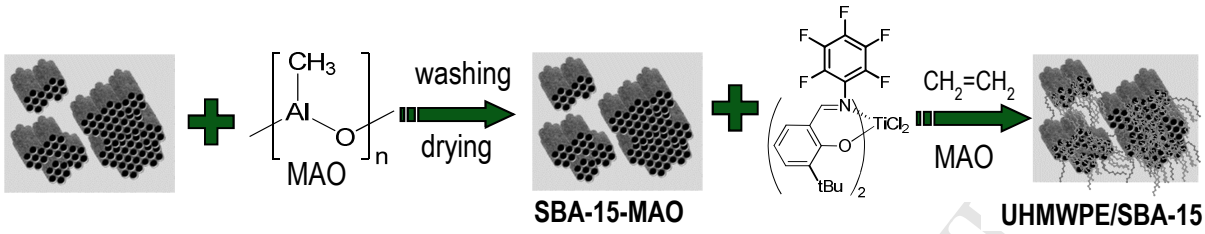

Scheme 3

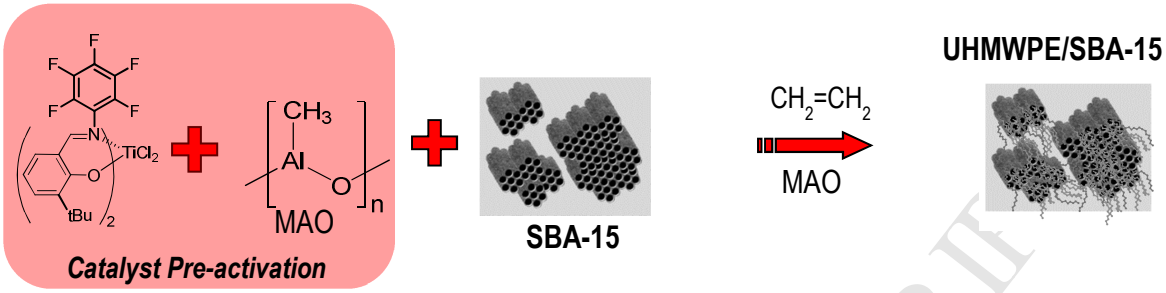

Scheme 4

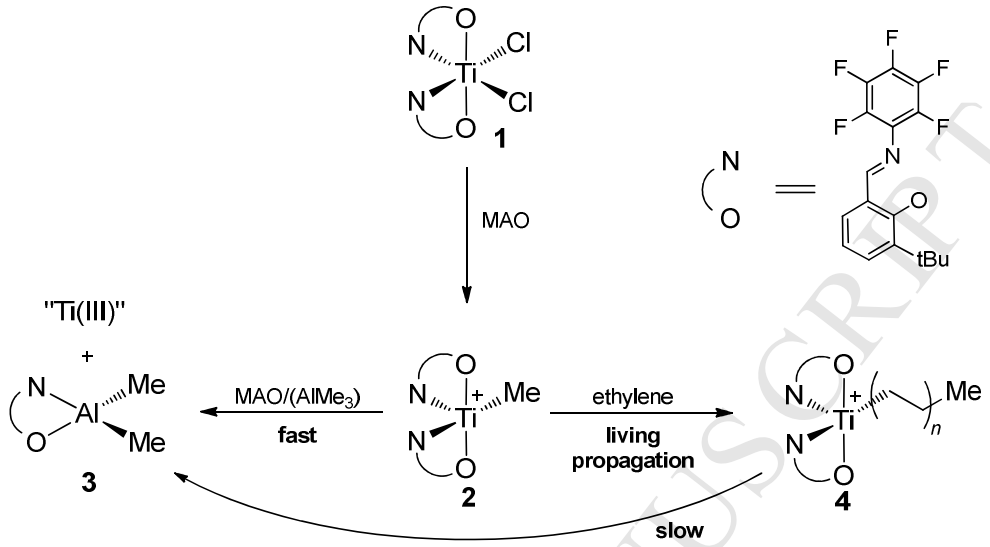

Figure captions

Figure 1: (a) SEM image (b) TEM micrographs of SBA-15.

Figure 2: Normalized kinetic profiles for ethylene polymerizations.

Figure 3: SEM micrographs for the FIHOM002 homopolymer and FISBA007 and FISBA017 composites at different magnifications.

Figure 4: TGA curves of neat UHMWPE (left) and its nanocomposites (right) under inert (top) and oxidative atmosphere (bottom).

Figure 5: DSC curves of the first melting (a and b) and subsequent crystallization processes (c and d) of neat UHMWPE and nanocomposites. Melting region of the small crystallites in the inset

Figure 6. Stress-strain curves for different homopolymers and composites: at 25 ℃ (left) and 90 ℃ (right).

Figure 7: Indentation curves of load-maintenance-unload vs. depth for some homopolymers (left) and composites (right).

Figure 8: Indenter depth dependence on experimental time for some homopolymers (top curves) and composites (bottom curves).

Table captions

Table 1: Polymerization conditions, activities, productivities, molar mass and dispersities for the UHMWPE's attained under homogenous conditions.

Table 2: Polymerization conditions, activities, productivities, molar masses and dispersities obtained for the polymeric materials attained with the supported catalyst.

Table 3: Average SBA-15 wt. % content, characteristic decomposition temperatures under nitrogen and air atmospheres for neat UHMWPE specimens and nanocomposites (the temperatures of 5%, $T_{5\%}$, and 50%, $T_{50\%}$) and the SBA-15 wt.% content at a specific environment.

Table 4: SBA-15 wt.% content, crystallinity values of films from X ray experiments and DSC calorimetric data for neat UHMWPE and nanocomposites (films and powders from the reactor).

Table 5: Mechanical parameters of different samples, analyzed at 25 ℃ and at 90 ℃: Young's modulus, E; average value. $E^{average}$; yield deformation, ε_Y; yield stress, σ_Y; final stress, σ_{end}.

Scheme Captions

Scheme 1: The FI catalyst used.

Scheme 2: Impregnation of catalyst on SBA-15 previously modified with MAO.

Scheme 3: Impregnation on SBA-15 support of pre-activated catalyst with MAO.

Scheme 4: Proposed pathways for the reaction of the FI catalyst with MAO. Reprinted with permission from [35]. Copyright (2015) American Chemical Society.

Sample	Al/Ti	Reaction time (min)	Average activity (kgPE/molTi.h)	Productivity (kgPE/molTi)	M_w (10^6 g/mol)	M_w/M_n
FIHOM014	500	6.5	17660	2019	1.045	n.a
FIHOM003	1500	6.5	19730	2140	-	--
FIHOM004	1500	13	19150	4150	1.479	n.a.
FIHOM008	2500	6.5	20380	2210	1.172	1.3
FIHOM002	2500	13	19310	4180	1.359	1.5
FIHOM018	2500	26	14580	6308	2.033	1.6
FIHOM005	5000	6.5	21380	2316	1.197	1.4
FIHOM007	5000	26	15150	6565	1.881	n.a.

Sample	Method	FI load in the support (10^{-6} mol/g)	Impreg-nation time (min)	Al/Ti	Reaction time (min)	Average activity (kgPE/ mol Ti.h)	Produc-tivity (kgPE/ molTi)	M_w (10^6 g/mol)	M_w/M_n
FISBA007	SBA-MAO	19	4	2500	12	3160	632	0.541	2.2
FISBA004	SBA-MAO	19	60	5000	153	380	960	0.590	1.6
FISBA003	SBA-MAO	19	180	2500	146	220	696	0.339	2.6
FISBA016	PA	8	90	1250	9	8120	1305	1.965	1.9
FISBA017	PA	8	90	2500	15	5460	1364	0.838	2.5

Sample	Average SBA-15 wt.% content	Inert atmosphere			Oxidative atmosphere		
		$T_{5\%}$	$T_{25\%}$	SBA-15 wt.% content	$T_{5\%}$	$T_{25\%}$	SBA-15 wt.% content
FIHOM014	0	435	461	0	269	400	0
FIHOM004	0	398	447	0	278	397	0
FIHOM002	0	421	455	0	282	364	0
FIHOM005	0	429	456	0	288	400	0
FISBA007	5.8	415	442	5.6	290	407	6.0
FISBA004	4.5	398	428	5.2	289	403	3.8
FISBA016	6.9	437	461	6.8	273	364	7.0
FISBA017	8.5	413	441	8.4	270	310	8.6

Sample	SBA-15 wt.%^{TGA}	*Film*					*Powder*	
		f_c^{XRD}	f_c^m	T_m (ºC)	f_c^C	T_C (ºC)	f_c^m	T_m (ºC)
FIHOM014	0	0.60	0.51	130.0	0.55	116.5	0.82	140.5
FIHOM004	0	0.56	0.52	131.5	0.54	118.0	0.82	140.0
FIHOM002	0	0.58	0.53	131.0	0.54	118.0	0.83	140.5
FIHOM005	0	0.59	0.51	131.5	0.56	117.5	0.82	140.5
FIHOM007	0	0.51	0.48	131.5	0.51	118.0	0.81	141.0
FISBA007	5.8	0.50	0.49	130.0	0.49	117.5	0.78	141.0
FISBA004	4.5	0.44	0.57	133.0	0.56	118.5	0.82	142.0
FISBA016	6.9	0.46	0.49	132.5	0.47	118.0	0.78	140.5
FISBA017	8.5	0.48	0.49	132.5	0.46	118.5	0.77	139.5

Sample	SBA-15 wt.%	$E^{average}$ (MPa)	ε_Y (%)	σ_Y (MPa)	σ_{end} (MPa)
T = 25 ℃ at 1 mm/min					
FIHOM002	0.0	227	50	18.2	21.6
FIHOM004	0.0	230	50	18.4	22.8
FISBA004	4.5	262	48	19.9	31.3
FISBA016	6.9	326	35	20.7	33.5
T = 90 ℃ at 1 mm/min					
FIHOM004	0.0	60	42	5.5	8.1
FISBA016	6.9	107	38	6.7	9.8

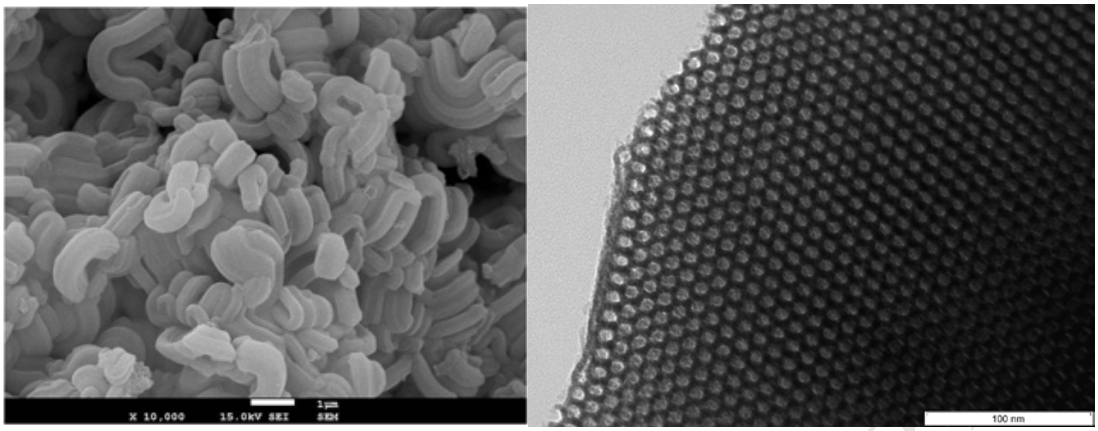

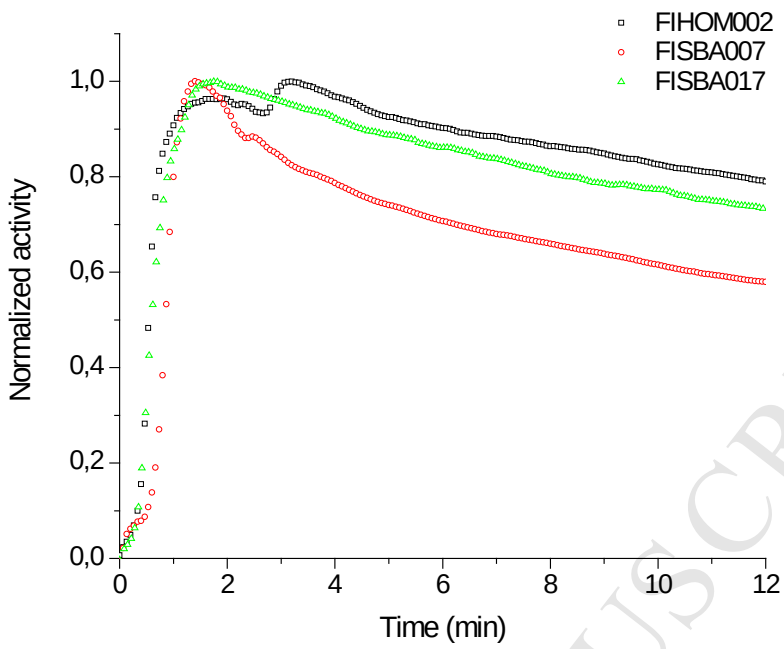

FIHOM002

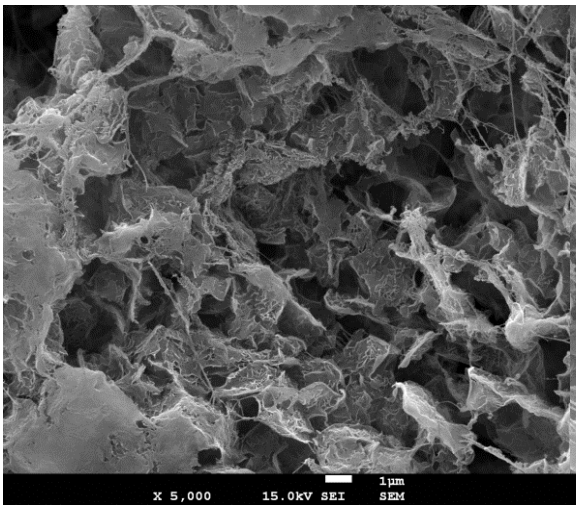

FISBA017

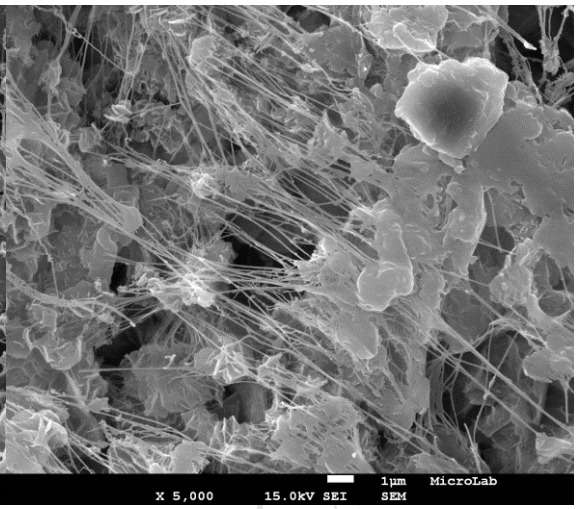

FISBA007

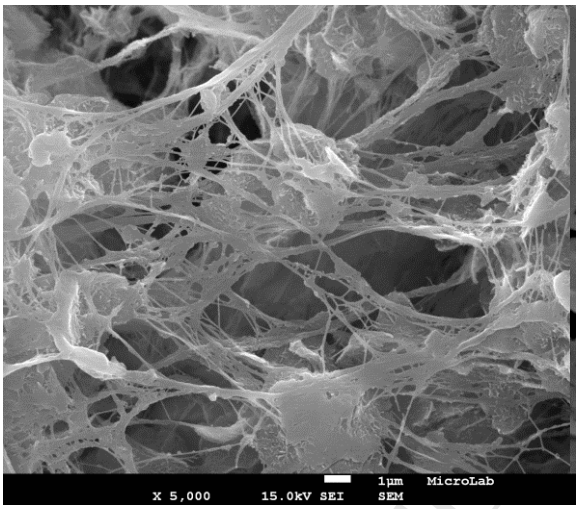

FISBA007

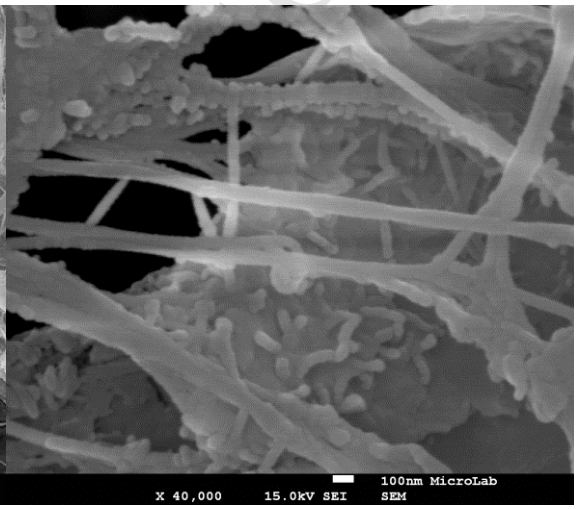

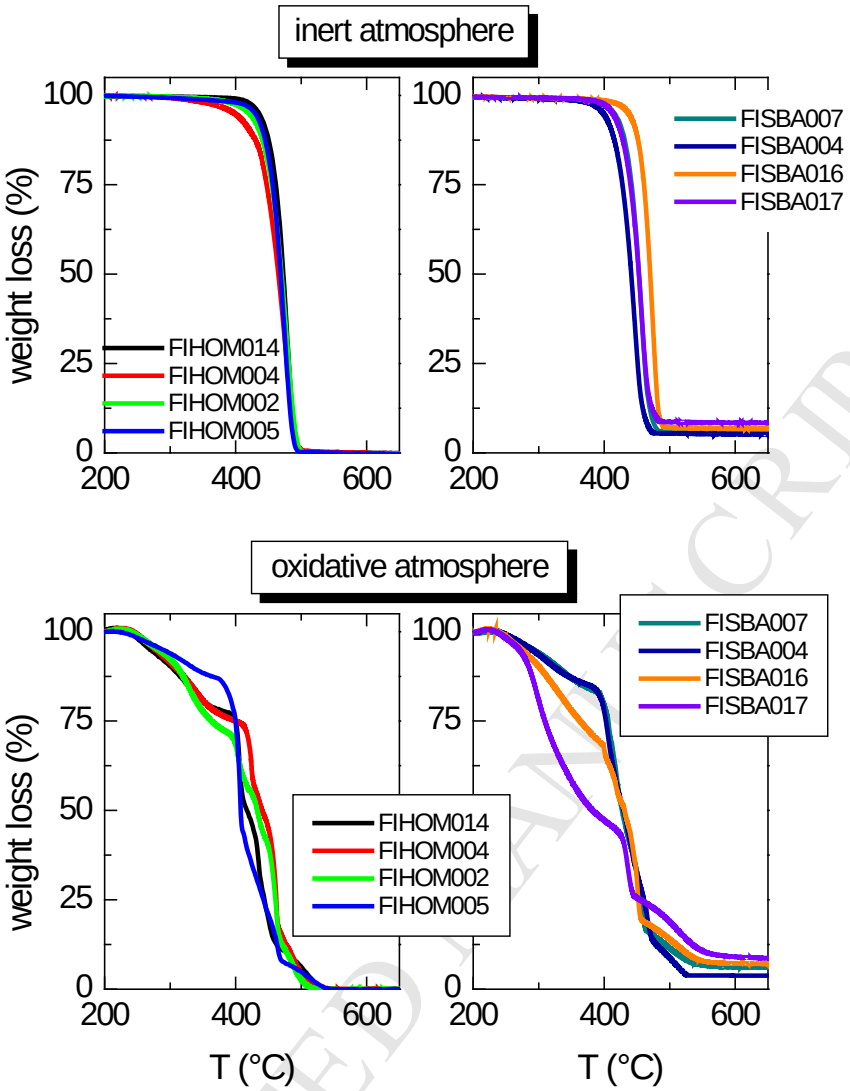

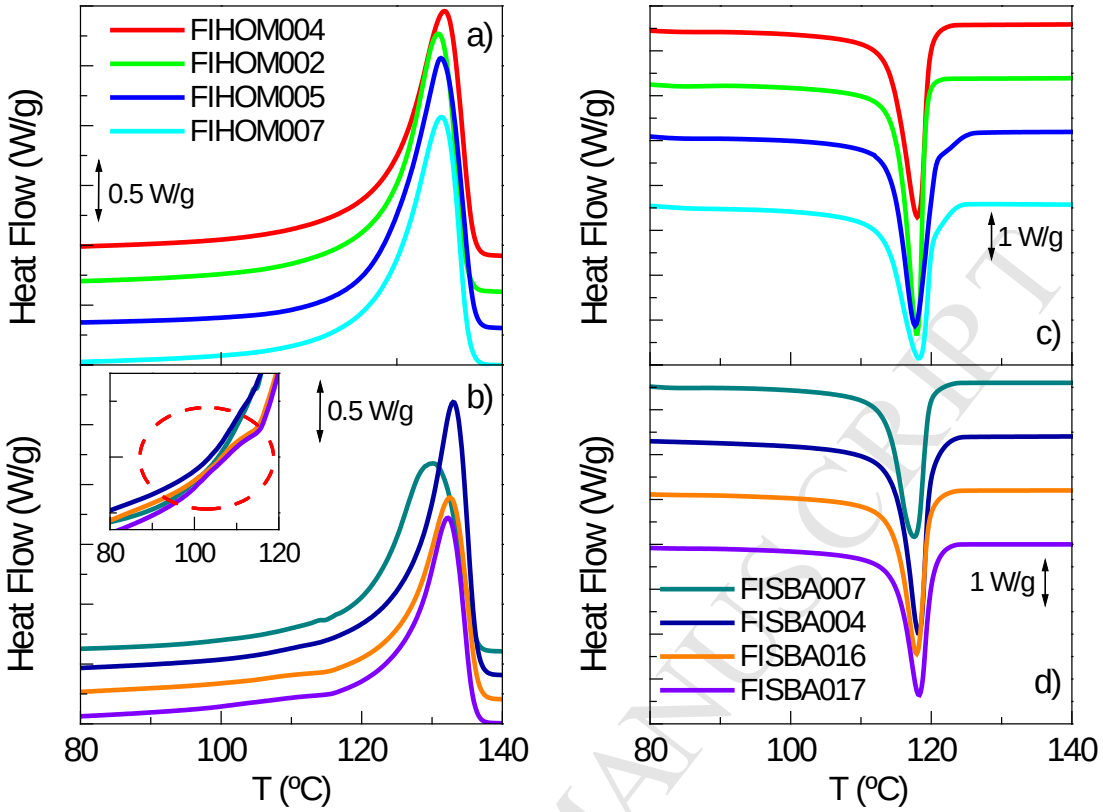

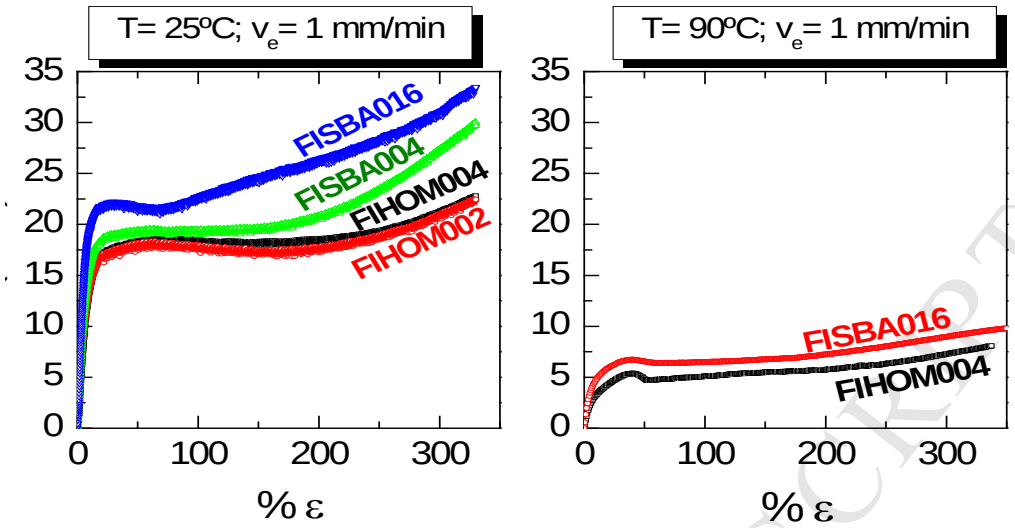

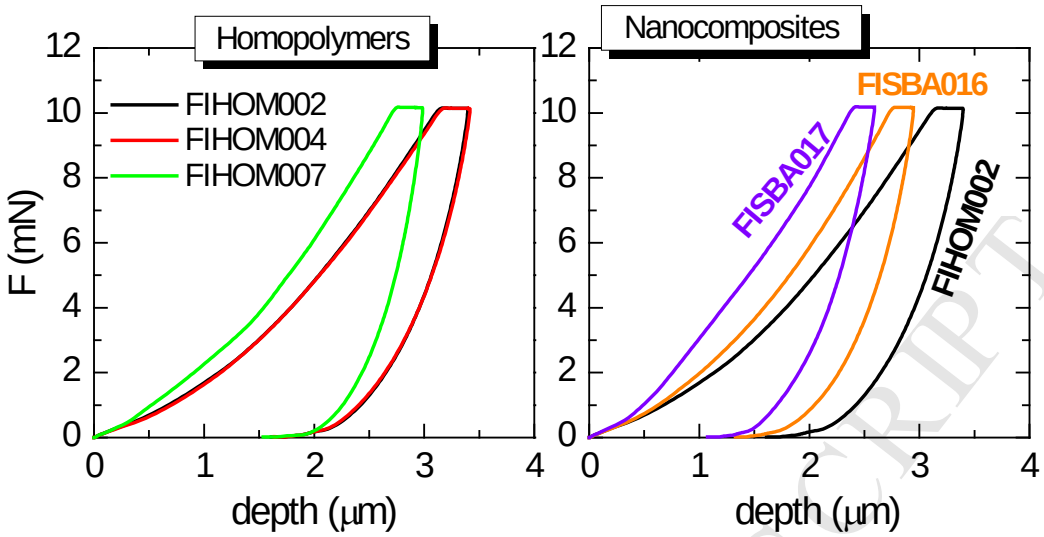

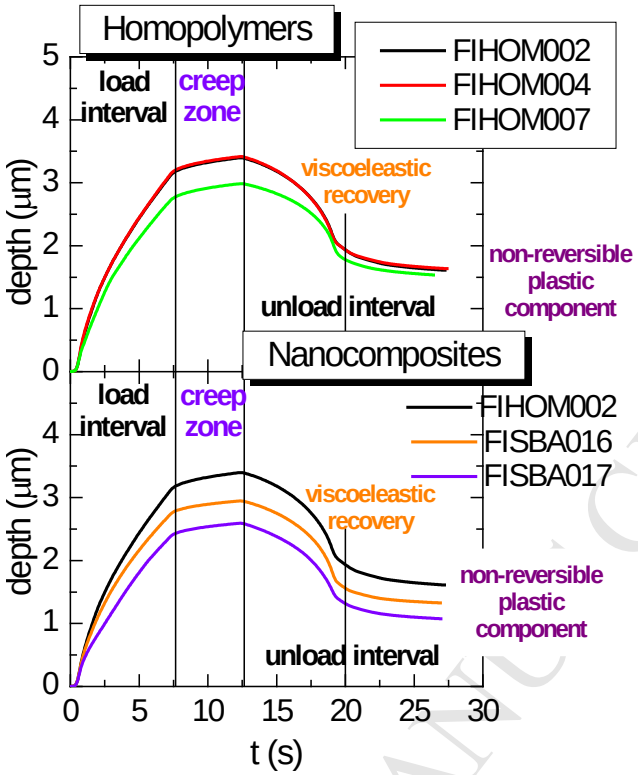

- Optimized immobilization methodology for FI catalyst on SBA-15 ordered porous silica allows attaining high polymerization activities and very high polymer molar masses.
- UHMWPE/SBA-15 nanocomposites have been synthesized by *in situ* polymerization.
- Stiffer materials are obtained with higher elastic modulus, mechanical strength and toughness compared with those found in the neat UHMWPEs.